Nuclear Inst, and Methods in Physics Research B 415 (2018) 72–81

Contents lists available at ScienceDirect

Nuclear Inst. and Methods in Physics Research B

journal homepage: www.elsevier.com/locate/nimb

Production of intensive negative lithium beam with caesium sputter-type ion source

Nikolai R. Lobanov

The Department of Nuclear Physics, Research School of Physics and Engineering, The Australian National University, Canberra, Australia

ARTICLE INFO

Keywords:
Negative ions
Sputter sources
Negative lithium beams

ABSTRACT

Compounds of lithium oxide, hydroxide and carbonate, mixed with silver, were prepared for use as a cathode in caesium-sputter ion source. The intention was to determine the procedure which would produce the highest intensity negative lithium beams over extended period and with maximum stability. The chemical composition and properties of the samples were analysed using mass-spectrometry, optical microscopy, Scanning Electron Microscopy (SEM), Energy Dispersive X-ray Analyses (EDX) and Raman spectroscopy. These analyses showed that the chemical transformations with components resulted from pressing, storage and bake out were qualitatively in agreement with expectations. Intensive negative lithium ion beams > 1 μA were delivered using cathodes fabricated from materials with multicomponent chemical composition when the following conditions were met: (i) use of components with moderate enthalpy of formation; (ii) low moisture content at final stage of cathode production and (iii) small concentration of water molecules in hydrate phase in the cathode mixture.

1. Introduction

Ion sources that produce negative ion beams are essential for the operation of tandem electrostatic accelerators in applied and basic research programs [1,2]. For example, lithium ion beams produced with tandem accelerators and cyclotrons [3] are used in the study of alpha-particle transfer reactions. The EXCYT project (Exotics with Cyclotron and Tandem) at the Istituto Nazionale di Fisica Nucleare (INFN-LNS, Italy) can deliver radioactive ^{8}Li beams using a positive ion source coupled to a Charge Exchange Cell (CEC). At the Australian National University (ANU), coincidence measurements imposed on the breakup fragments, at sub-barrier energies, following the reaction of ^{6,7}Li with ^{208}Pb have enabled the complete characterisation of the breakup processes. The ^{6,7}Li beams, from the 14UD electrostatic accelerator, were used with 98.7% enriched ^{208}PbS targets [4].

Over the years, many different devices for negative lithium ion production have been developed. A Penning discharge source supported by a Ne-H_2 mixture into which Li is evaporated is described in [5]. A 500 nA beam current of LiH_2^- could be sustained for many hours. A positive ion source with a CEC on the extraction side [6] offers a universal method of producing μA quantities of beams. Sources of this type are complex, difficult to operate and have a shorter life compared with Cs sputter ion-sources, the recent technical developments of which have expanded their capabilities and flexibility [7,8]. With appropriate cathode materials, these sources can produce intense beams throughout the periodic table [9–11]. Currently on-going international efforts have focussed on increasing the source output and efficiency and to better control Cs in order to reduce its consumption and significantly extend the time between maintenance cycles [12–15].

In the case of negative lithium beams produced with Cs sputter ion-sources, an obvious cathode choice is Li metal, however, this has been found to be generally unsatisfactory [16]. The initial several μA of negative Li ion current usually reduced to ~100 nA after 30 min of operation. The early high Li current was due to the surface oxide layer and once sputtered away the negative output fell rapidly. Better results were obtained by bleeding O_2 over the Li metal surface. The outcomes were unreliable. In addition, the reactive nature of metallic Li caused difficulties during sample preparation and handling.

The use of various chemical mixtures as cathode fill material proved to be more effective [16]. The cathodes were prepared from lithium hydride LiH, lithium amide $LiNH_2$, fluoride LiF, sulphide Li_2S and lithium nitride Li_3N. The first four performed satisfactorily, but the Li^- currents were low. The Li_3N performed much better producing steady currents in the a few μA range. Unfortunately, lithium nitride is highly flammable and corrosive, requiring careful handling, and should be avoided, if possible.

The best reported results were attained using Li metal burnt by igniting it with a propane torch [16]. Further heating melted the residue into a ball of clear liquid that turned white on cooling. It was assumed that the end product was LiOH since the melting point of Li_2O was 1700 °C and that of LiOH was 450 °C. The cold pellet was rapidly crushed, mixed with silver powder and pressed into a cathode. The

E-mail address: nikolai.lobanov@anu.edu.au.

https://doi.org/10.1016/j.nimb.2017.11.004
Received 1 June 2017; Received in revised form 3 November 2017; Accepted 3 November 2017
Available online 14 November 2017
0168-583X/

promptness was important due to hydroscopic nature of LiOH. The fresh cathode produced a few μA of lithium beam for up to ~8 h.

The production of negative Li beams based on the use of lithium oxide or carbonate in conventional sputter-type ion sources was described in [17]. The selected sputter raw materials were Li-Cu alloys in 1:1 proportion. The initial results proved to be poor, yielding negative Li beam intensities of only few nA. Exposure the Li-Cu samples to ambient for extended periods of time caused the conversion from Li-Cu to Li_2O-Cu. As a result, the beam output grew up to a few μA at a sputter probe voltage ~3 kV. These results suggested potentially good performance with mixtures of Li_2O and Cu or Ag powder. Since the oxides of the alkali metals (IA) group are highly deliquescent, presenting problems during cathode fabrication and storage, the carbonate of group IA would be less hydroscopic and easier to press into a cathode and to handle. The Li_2CO_3 was mixed with ~10% (atomic) Cu powder and pressed into a cathode. The negative Li beam current was in excess of 0.5 μA with a lifetime > 40 h.

The results, obtained from use of Li_2O mixed with Ag powder, were reported through the Symposium of Northeast Accelerator Personnel (SNEAP) discussion forum [18]. The main developments could be summarised as follows: (i) a few μA of negative lithium beam was produced when cathodes were pressed from fresh (recently bought) Li_2O mixed with Ag; (ii) older cathodes stored under ambient conditions performed poorly probably due to moisture and CO_2 absorption. Another successful method as discussed through SNEAP forum was to bake the cathodes in vacuum at 200 °C for > 4 h and to cool them down in vacuum. Afterwards, the cathodes were transferred to a storage container filled with argon where they were kept until use. According to another SNEAP communication, high negative lithium currents were observed when the cathodes were baked in vacuum at 100 °C for one hour or in a furnace at ambient atmosphere, at the same temperature, for two hours.

The main focus here is on experimental verification and phenomenological elucidation of optimal procedures to prepare cathodes capable of producing μA quantities of negative lithium beams with sputter-type ion sources. The paper has been organised into three main sections. The Section 2 outlines the general concept of cathode fabrication and introduces the experimental procedures, tailored for multi-component chemical mixtures, for pressing and handling. A number of characterisation techniques suitable to evaluate the chemical mixtures are described. Section 3 presents key experimental results based on characterisation techniques including mass-spectrometry, optical microscopy, SEM/EDX and Raman spectroscopy used to collect information about the properties of lithium-based chemical mixtures and their transformations during the process. Section 4 includes the interpretation of the experimental results in relation to the output of negative Li ion-beams. Potential developments that would help to improve the ion source performance are also discussed.

2. Methods

2.1. Cathode preparation procedures

The standard cathode geometry is a cylinder 7.8 mm in diameter and 20.8 mm long. These are made of C11000 Electrolytic Tough Pitch (ETP) copper alloy, as per drawing, shown in Fig. 1(a). For expensive isotopic mixtures, the D = 3.3 mm diameter by H = 5 mm deep hole in the front is drilled to only 1.5 mm in diameter by 1.0 mm deep.

The surface treatment of the cathodes after fabrication is important and utilised the following steps. After three immersions into a vapour degreaser, the parts are cooled to room temperature. Once cooled, the parts are soaked and washed in a clean alcohol bath. The next step is to soak in sulfamic acid, which acts as a cleaning and descaling agent. Finally, the cathodes are rinsed and soaked firstly in 5% citric acid for passivation and secondly rinsed in deionised water. As soon as parts are dry, the cathodes are stored in plastic containers in ambient conditions. A few cathodes are left in the oven at elevated temperature of 60 °C for immediate use. A limited number of short cathodes are manufactured (7.8 mm in diameter and 6.0 mm long) to fit into sample stages of the characterisation equipment.

Powders, used in compressed mixtures, often benefit by the addition of a binder in order to increase their compacting properties and electrical conductivity. Fine aluminium, copper or silver powders are commonly used with particle sizes ranging from few μm up to tens of μm. The choices of binding metal and mixture composition are based on the following considerations: (i) the base and binding materials should have similar sputtering yields, (ii) be comparable in particle size, (iii) the binding materials should have low electron affinity and (iv) the mixture should contain similar quantities of atoms in base and binding constituents.

Two following powder mixing techniques were employed in this study: (1) powders placed at the bottom of a chemical dish were mixed using a spatula and (2) they were further ground into a final fine powder composition within a porcelain mortar and pestle. Both the pestle and the exterior of the mortar were made of glazed porcelain. The mortar's interior was unglazed for more effective grinding.

The cathode pressing involved compression of a free flowing powder mixture in the enclosed cylindrical cavity of the cathode. The compression was applied in a uniaxial direction by a punch (b) entering the die (a). The punch was made from hardened tool steel and its surface was ground and polished on the impacting surfaces. The clearance between the punch and die was less than 0.05 mm. The cathode was inserted in a split steel housing (c). The role of the housing was to provide alignment between the punch and the die and to stabilise the cathode's geometrical shape, which could be affected by application of a strong compressional force. The completed system utilised a small mechanical press with capacity up to 25 tonnes as shown in Fig. 1(d).

The powder mixture as dispensed into a cathode (die) is composed of solid particles and pores. The ratio of the powder mass to the volume of the die is called the poured bulk density ρ_P. Mechanical tapping or vibrating of the cavity rearranges the particles causing collapse and displacement of the pores. The degree of rearrangement depends on particles size, shape and surface roughness. The tapped density ρ_T is an increased bulk density attained after tapping is completed. The ratio ρ_T/ρ_P is known as Hausner ratio H and it characterises the ability of powder to flow. A similar parameter is the Carr's index given as $100(\rho_T - \rho_P)/\rho_P$. The three main mechanical properties which play a key role in the compression process are: fragmentation, plastic and elastic deformation. Fragmentation involves the breaking up of the particles into separate clumps. Plastic deformation is a permanent change, while elastic deformation describes restoration of original form after the force is removed. Plastic deformation is observed up to the compression pressure, where porosity is reduced below 10% [19], when pores are nearly eliminated, and further compression is controlled by elastic deformation. The relationship between the volume of a powder in a die and the force needed to attain this volume is a characteristic of the mechanical properties of the powder. Ideally, the density increase should occur uniformly throughout the compacted powder. However, in geometries with low aspect ratio D/H < 1, variations in density can be significant mainly due to friction between powder particles. Better uniformity can be achieved through multiple pressings by adding more powder at a time.

As an example, let's consider the cathode preparation from Li_2O with Ag binder. Mixing the ingredients by weight in proportion 22% Li_2O with 78% Ag will result in a similar number of atoms of both components. The Hausner ratio for this powder mixture can be obtained my measuring the poured and tapped volumes, according to formula $H = \rho_T/\rho_P = V_P/V_T = 36.5/23.52 = 1.55$, where $V_P = 36.5\,mm^3$ and $V_T = 23.52\,mm^3$ are poured and tapped volumes occupied by the powder. The Carr's ratio is calculated by the formula $C = 100(V_P\text{-}V_T)/V_T = 35.5\%$. Hausner ratio bigger than H > 1.25 and Carr index greater than C > 25% indicates poor flow-ability of mixture under investigation [19].

Fig. 1. Cathode pressing tools and equipment: (a) cross-section of cathode blank made of C11000 ETP copper; (b) punch made from hardened tool steel; (c) assembled split housing holding the cathode (top) and with top plate and punch inserted (bottom) and (d) complete pressing installation.

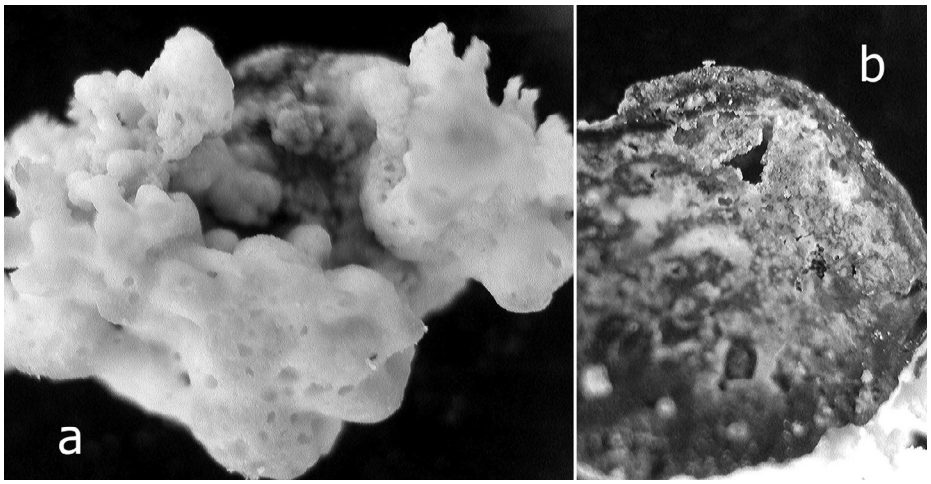

Fig. 2. Reaction products of lithium burnt in air include a white coralline material (a) and dense black crystals underneath (b). The combustion of lithium in air is illustrated in the linked video.

Table 1
Chemical reactions occurring during processing and handling of lithium based chemicals.

N	Chemical equation	Temperature, °C	Li metal	Li_2O	LiOH	Li_2CO_3
1	$4Li + O_2 \rightarrow 2Li_2O$	200	✓			
2	$2Li + 2CO_2 \rightarrow Li_2C_2 + 2O_2$	200	✓			
3	$2Li + 2CO \rightarrow Li_2C_2 + O_2$	200	✓			
4	$6Li + N_2 \rightarrow 2Li_3N$	200–250	✓			
5	$Li_2C_2 + 2H_2O \rightarrow 2LiOH + C_2H_2$	20				
6	$2Li_2C_2 + 5O_2 \rightarrow 2Li_2O + 4CO_2$	500	✓			
7	$Li_2C_2 \rightarrow 2Li + 2C$	1000	✓			
8	$Li_2O + H_2O \rightarrow 2LiOH$	20		✓		
9	$Li_2O + CO_2 \rightarrow Li_2CO_3$	500–600	✓			
10	$2LiOH + CO_2 \rightarrow Li_2CO_3 + H_2O$	20		✓	✓	
11	$LiOH + H_2O \rightarrow LiOH \cdot H_2O$	20		✓	✓	
12	$2LiOH \rightarrow Li_2O + H_2O$	800–900	✓			
13	$Li_2CO_3 \rightarrow Li_2O + CO_2$	1000	✓			✓
14	$Li_3N + 3H_2O \rightarrow NH_3 + 3LiOH$	20				
15	$2Li_3N \rightarrow 6Li + N_2$	300–500	✓			

Table 2
Electron affinities (E_A) of selected atomic species and molecules.

Element	H	Li	C	O	OH	C_2	O_2	CO_2	Ag
E_A, eV	0.754	0.618	1.262	1.461	1.827	3.269	0.45	1.11	1.302

2.2. Components used for production of negative lithium beams

In the present work the materials were limited to the following chemicals: (i) burnt lithium metal, (ii) lithium oxide, (iii) lithium hydroxide, (iv) lithium carbonate and (v) silver as a binding component.

The burnt Li_2O was prepared by placing a small piece of Li metal (few tens of mg) on a molybdenum sheet metal substrate inside a fume hood and igniting with a propane torch. The lithium burned, as shown in a video, linked to the Fig. 2 emitting intense white light and produced three types of residual products: a finely divided aerosol, a white crystalline deposit (a) and a dense dark lower layer (b), as shown in Fig. 2. The aerosol consisted of lithium oxide, hydroxide and carbonate. The white top layer contained mainly lithium oxide while the dark bottom layer was primarily lithium nitride and oxide [20]. The cooled crystalline deposit was crushed, mixed with silver powder and pressed into a cathode. The composition of the mixture was 22% Li_2O mixed with 78% Ag binder by weight. Pure silver powder (> 99.9%) with particle size of 5–8 μm was used as the binder metal.

In case of other materials, a 97% lithium oxide powder 60 mesh (250 μm), 99.95% crystalline lithium hydroxide and 99.5% lithium

Table 3
The standard enthalpy (heat) of formation $\Delta H_f^{\ominus}$, density ρ, melting temperature T_M and boiling temperature T_B of chemical mixtures used for production of negative lithium beams.

Component	Li_2O	Li_2C_2	Li_2CO_3	Li_3N	LiOH	$LiOH \cdot H_2O$	H_2O
$\Delta H_f^{\ominus}$, kJ/mol	−595.8		−1215.6	−164.6	−606.2	−487.5	−242.0
ρ, g/cm^3	2.013	1.3	2.11	1.27	1.46	1.51	0.995
T_M, °C	1438	> 550	723	813	462	450–471	0
T_B, °C	2600		1310		924	924	100

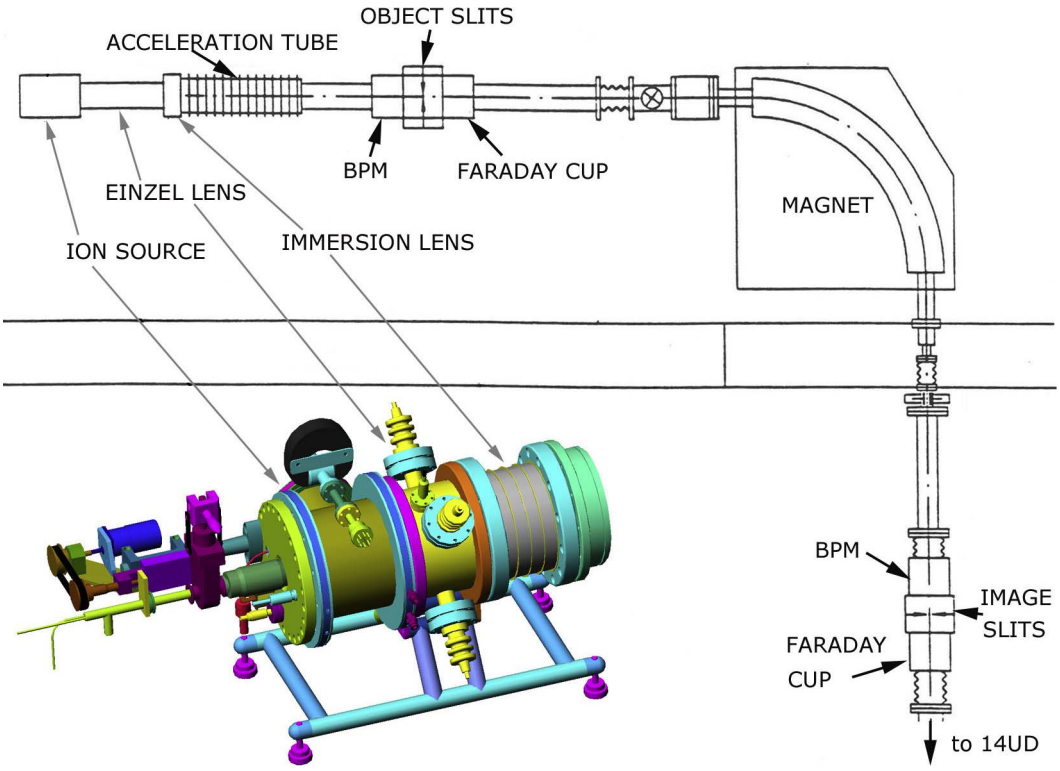

Fig. 3. A schematic drawing of the ion source facility used to measure mass spectra of the negative beams. Both object and image slit set at ± 1.2 mm for high resolution. The inset shows the rendered image of modified SNICS ion source.

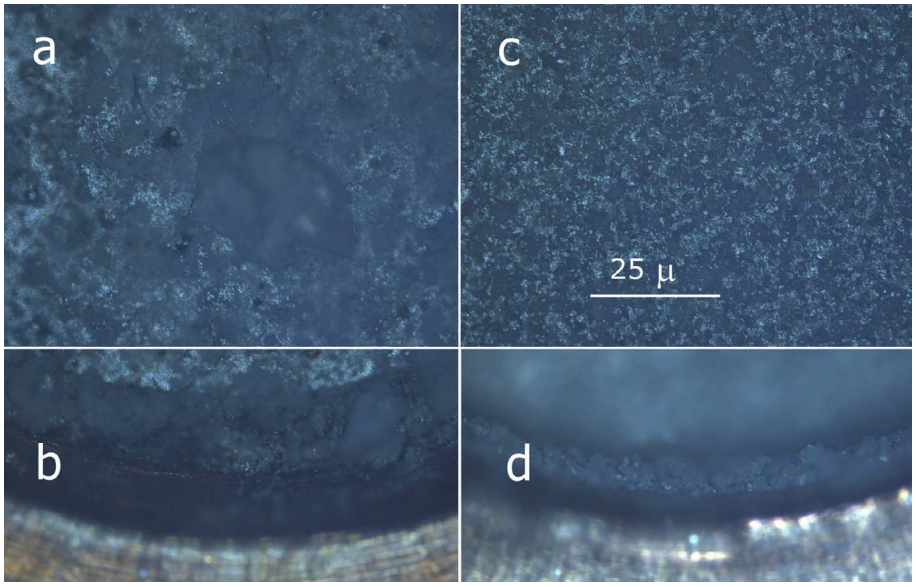

Fig. 4. Optical images of pressed cathodes made of 22% Li_2O with 78% Ag binder by weight: (a) premixing was completed by spatula only; (b) same as (a) but acquired at the edge of cathode die and focused on transition between the die and compact; (c) premixing was accomplished by spatula followed grinding up by mortar and pestle; (d) same as (c) but at the edge of cathode die focusing on transition between the die and compact. Images were produced with optical microscope Leica DM 4000M.

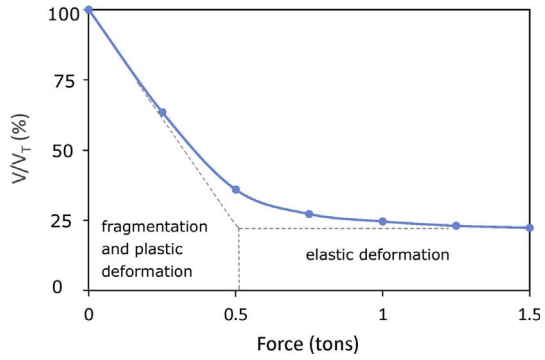

Fig. 5. Volume-force relationship during compacting 22% Li_2O with 78% Ag powder mixture. The plotted data is presented as a ratio of volume V to known tapped volume V_T. The compressive strain in the punch is ignored.

carbonate were also used to make test cathodes. All materials were purchased from Aldrich and used without further purification.

2.3. Post-pressing procedures

Laboratory powders often contain moisture that is in thermodynamic equilibrium with the atmosphere. As a consequence, the composition of the sample depends on the relative humidity and ambient temperature at the time it is pressed. To cope with this variability, it is desirable to reduce sample moisture levels. In solid powders, the water can be present in an essential or nonessential form. In essential form water is an integral part of the molecular structure of the compound in its solid state. For example, water molecules in a stable solid hydroxide monohydrate $LiOH \cdot H_2O$ qualify as an essential water. Nonessential water is retained by solids as a consequence of physical forces. Adsorbed water is a type of nonessential water that is retained on the surface of solids and is held as a condensed phase in the interstices or capillaries of a colloidal solid. Occluded water is entrapped in microscopic pockets spaced irregularly through solid crystals. Such cavities often occur in pressed powders. In general, the concentration of water in a solid tends to decrease with increasing the temperature and decreasing humidity. Most hydrated compounds can be converted to the anhydrous form by oven drying at 100–120 °C for a couple of hours. The amount of water absorbed in a solid generally approaches zero when the solid is heated above 100 °C. As indicated by drying curves for chemical compounds, the weight stabilizes after 70 min at 105 °C [21]. The occluded water is not in equilibrium with the atmosphere and is insensitive to changes in humidity. Heating a solid containing occluded water may cause a gradual diffusion of the moisture to the surface where it evaporates. Sometimes, during heating, the solid crystals are suddenly shattered by the steam pressure created from moisture trapped in the internal cavities. In this work the pressed cathode was dried by heating the sample in a conventional oven above 150 °C for a couple of hours, just before it was installed in the ion source. While this procedure may not completely remove the moisture, it was usually lowered it to a reproducible level.

2.4. Basic chemical reactions occurring during processing and handling of cathode mixtures

Main reactions relevant to chemical transformations during processing and handling of cathode mixtures are presented in Table 1 [22].

The chemical reactions relevant to substances under investigation are marked with a tick symbol. For example, in case of burnt lithium metal, the anticipated chemical composition of cathode mixture is Li_2O with traces of Li_2C_2 and Li_2CO_3 according to reactions (1)–(4), (6), (7), (9), (12), (13) and (15). When exposed to ambient conditions, for a long time, the mixture will be enriched with LiOH and Li_2CO_3 due to reactions (5), (8) and (10). Following burning of lithium metal, some amount of lithium atoms could remain in the mixture due to incomplete burning and decomposition of Li_2C_2, as per Eq. (7) or Li_3N, Eq. (15). Therefore, after the bake out the expected chemical composition of burnt lithium metal is dry Li_2O with traces of Li_2CO_3 and Li_3N, as per Eqs. (1), (2), (4) and (15).

In case of Li_2O, stored under ambient conditions, the anticipated composition of the mixture is Li_2O, LiOH, $LiOH \cdot H_2O$ and Li_2CO_3 through the reactions described by Eqs. (8), (10) and (11). After the bake out, the expected chemical state of the same sample is mainly dry Li_2O with traces of Li_2CO_3. The lithium hydroxide monohydrate will be dehydrated.

When using LiOH, under ambient conditions in presence of moisture, the LiOH should contain traces of Li_2CO_3 and $LiOH \cdot H_2O$, as per reactions (10), (11). After the bake out is completed, the expected chemical composition of the same sample will be mainly dry LiOH with traces of Li_2CO_3. The lithium hydroxide monohydrate will be dehydrated.

2.5. Generation of negative ions with caesium sputter-type ion source (CSIS)

Sputtering from a surface covered with a layer of Cs has proven to be an effective method of generating negative ion beams. Sputtering is caused by cascade momentum transfer between recoil atoms through the interaction with energetic projectiles leading to the expulsion of surface atoms. The electron affinity E_A characterises the negative-ion state or the binding energy of the additionally attached electron. In addition to atomic species, many molecular negative ions have been observed. The electron affinities of selected atomic species and molecules, relevant to this study, are shown in Table 2.

The pressed cathode powder mixture consists of grains with different composition and crystal structure. If a multicomponent surface is subjected to ion bombardment, the different components are sputtered at variable rates due to preferential sputtering [23]. High vapour pressure compounds, studied in this work, respond in specific ways to sputtering by ion bombardment. For example, molecular species or oxides may constitute a large fraction of the ions. Differences in the surface binding energy of the constituents results in preferential emission of the component with the lower binding energy. One component may be also enriched on the surface due to surface segregation and it will then be preferentially removed by sputtering. The sputtering

Table 4
Negative ion spectrum obtained from different cathode mixtures.

Composition, wt%	Baking	^{1}H, %	^{7}Li %	^{12}C %	^{16}O %	^{17}OH %	^{63}Cu %	^{107}Ag %
22%Li_2O + 78%Ag	No	0.6	5.0	0.2	61	13.9	0.02	9.6
Solid Li burnt	Yes	0.5	4.0	0.4	66	8.8	0.27	10.0
22%Li_2O + 78%Ag	No	1.0	1.6	0.03	72	16.0	0.38	12.6
Li_2O powder	Yes	0.8	4.4	0.24	74	10.0	0.47	22.9
18%LiOH + 82%Ag	No	0.2	1.0	0.01	72	7.5	0.02	9.1
	Yes	1.4	11.	0.03	66	9.7	0.02	5.3
41%Li_2CO_3 + 59%Ag	No	0.2	1.6	0.7	74	6.8	0.55	15.5
	Yes	0.1	1.4	0.6	58	6.2	0.19	15.9

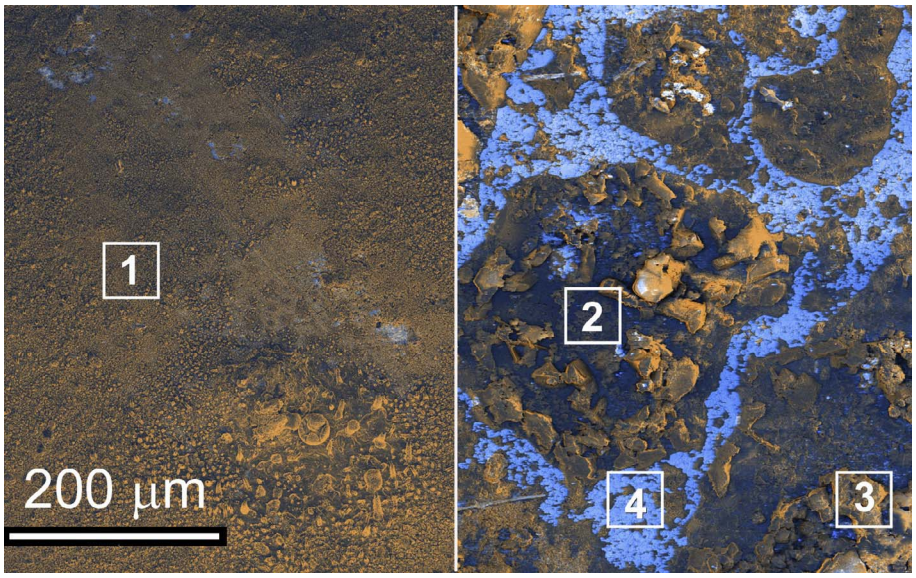

Fig. 6. SE/BSE image of 22%Li_2O + 78%Ag sample: unbaked (left) and baked (right). Lithium oxide is produced by burning of solid Li metal. Numbers in square boxes show the location of EDX analyses.

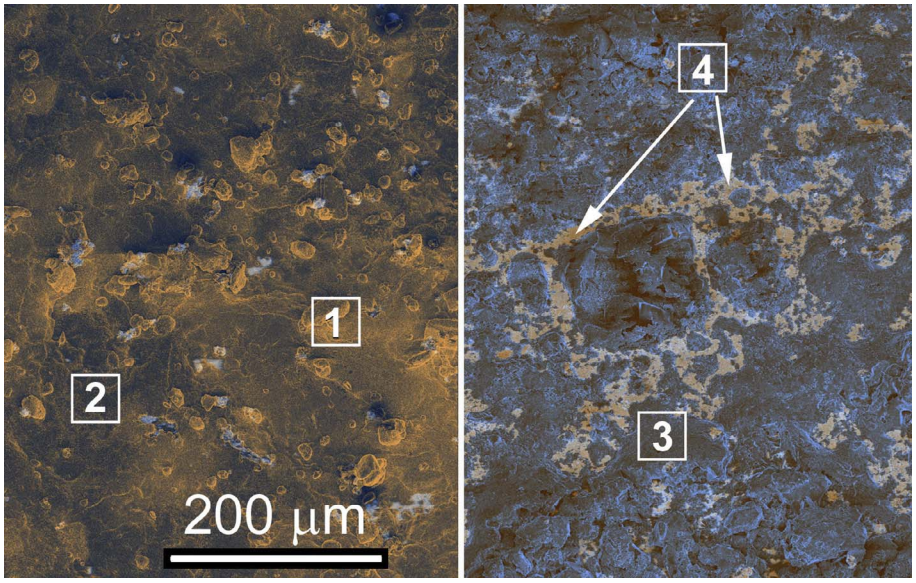

Fig. 7. SE/BSE image of 22%Li_2O + 78%Ag sample: unbaked (left) and baked (right). Commercial Li_2O powder is used. Numbers in square boxes show the location of EDX analyses.

process is controlled by the partial molar enthalpies of vaporisation of the various sputtered species. The standard enthalpies of formation of main cathode chemical components and some other physical properties are presented in Table 3.

Following previously published recommendations [23], it can be assumed that the negative ion yields are proportional to the partial sputter yield and depends upon the electron affinity of the sputtered components and possibly upon other parameters.

A theory of CSIS ionization, described in [24], is based on collision-radiation model of the caesium plasma that forms within a pitted sample region in which excited states of Cs are formed. The excited states of neutral Cs undergo Resonant Electron Transfer (RET) with neutral sputtered atoms resulting in production of negative ions. Many previously reported experimental observations, reviewed in [24], have been explained by RET phenomenon. The important conclusion of RET model relevant to this study is that the sample holder and binder substance should be made of materials with E_A lower than the sample component. Otherwise the anion yield of desired element will decline due to competition for excited states by different sputtered elements with similar E_A. For example, lithium has an E_A of 0.618 eV, therefore silver binder with E_A of 1.302 eV places it in competition for Cs(7d) state [24]. A better choice might be employing binding materials with lower E_A such as aluminium with E_A of 0.441 eV or niobium, E_A = 0.89 eV. In this study however, the silver has been selected due to its chemical stability during prolonged bake out.

2.6. Characterisation techniques

In this work the mechanical and chemical properties of different cathode mixtures and their performance were investigated by the following four characterization techniques:

2.6.1. Optical imaging

The powder mixture homogeneity, its particles size and shape were determined by using an optical microscope Leica DM 4000M. This model featured an automatic illumination and contrast managers enhanced by constant colour intensity control with LED-technology.

2.6.2. Ion source mass spectrum

Measurements reported in this work were completed employing a modified Source of Negative Ions by Caesium Sputtering (SNICS) [14]. Additional improvements included a spherical ionizer and a

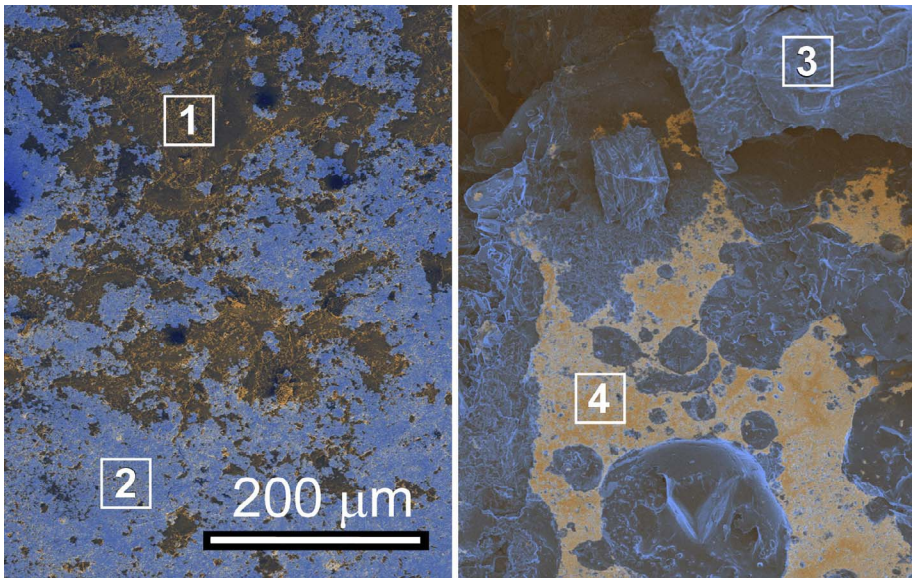

Fig. 8. SE/BSE image of 18%LiOH + 82%Ag sample: unbaked (left) and baked (right). Numbers in square boxes show the location of EDX analyses.

Table 5
A qualitative EDX analyses of the elements present in different cathode mixtures.

Composition, wt%	Baking	Fig.	Point (box)	C, wt%	O, wt%	N, wt%	Cu, wt%	Ag, wt%
22%Li_2O + 78%Ag	No	6	1	1.4	2.6	–	3.3	92.6
Solid Li burnt	Yes	6	2, 3	19.0	79.3	1.7	–	–
			4	6.3	28.4	1.6	–	63.7
22%Li_2O + 78%Ag	No	7	1, 2	9.5	60.2	–	0.9	29.4
Commercial Li_2O powder	Yes	7	3	20.8	79.2	–	–	–
			4	0.9	4.3	–	0.3	94.4
18%LiOH + 82%Ag	No	8	1, 2	1.0	3.8	0	2.6	92.6
	Yes	8	3	7.7	92.3	–	–	–
			4	4.2	22.8	–	2.3	70.7
Li_2O	No	–	–	3.1	96.9	–	–	–
	Yes	–	–	21.9	78.1	–	–	–
LiOH	No	–	–	3.4	95.0	–	1.1	0.4

distribution system for the caesium vapour, consisting of a confinement vessel between the ionizer and cathode [15].

A schematic of the SNICS ion source facility is shown in Fig. 3. The main low energy components are: decelerating Einzel lens followed by immersion lens, accelerating tube at 150 kV, remotely adjustable object slits, a combination of beam profile monitor (BPM) with electrically suppressed Faraday cup, 82.9 cm radius double focusing 90° dipole bending magnet, adjustable image slits, the second combination of BPM and supressed Faraday cup. The system is pumped by a combination of turbo and ion pumps to 10^{-8} Torr. The specifications of the sector bending magnet are: mass energy product 50 amu × MeV/Z^2; object slit distance (vortex) 2633 mm; image slit distance (vortex) 2433 mm and momentum dispersion 33 mm/%.

The typical cathode voltage was 5 kV. The ionizer power was in a range of 150–180 W. The caesium oven temperature was measured with a thermocouple and maintained to within 80 to 100 °C. The immersion lens voltage was set to ~13 kV, corresponding to a negative ion energy of 18 kV injected into accelerating tube to the final energy of 168 keV. The object and image slits were set at ± 1.2 mm.

2.6.3. SEM/EDX analyses

Scanning Electron Microscopy (SEM) and Energy Dispersive X-ray Analysis (EDX) can be used to image and investigate the properties and composition of a chemical mixture by (a) high resolution surface inspection and backscatter analysis of samples and (b) non-destructive, semi-quantitative elemental analysis of solids using energy dispersive X-ray microanalysis. Light elements with atomic number Z < 11 cannot be routinely analysed by EDX. Hydrogen (Z = 1) and He (Z = 2) do not have characteristic X-rays, and the Li (Z = 3) K X-rays are of too low energy to be detected by EDX. SEM FEI Verios was used featuring a field emission gun and a mono -chromator suitable for ultra-high resolution imaging. This instrument was equipped with an Oxford electron dispersive X-ray (EDX) spectrometer with an 80 mm^2 silicon drift detector.

2.6.4. Raman spectra analyses

Raman Effect is used as a powerful spectroscopic technique in chemical analyses of powder mixtures. In the Raman Effect, incident radiation is in-elastically scattered from a sample and shifted in frequency. The spectrum of Raman shifted light has several bands which can be related to a molecular structure. A Renishaw inVia Reflex Spectrometer System was used for Raman analysis of cathode samples. The system included a Peltier cooled CCD high efficiency spectrograph and a confocal inVia microscope with × 20 objective lens. A near infrared 785 nm wavelength excitation was selected as it performed efficiently for over 90% of Raman active materials with good balance of fluorescence reduction and spectral/spatial resolution. All Raman scans were completed under similar conditions: 3 extended scans over the range of 100 ÷ 3400 wave numbers at 0.5% of maximum laser power of 300 mW.

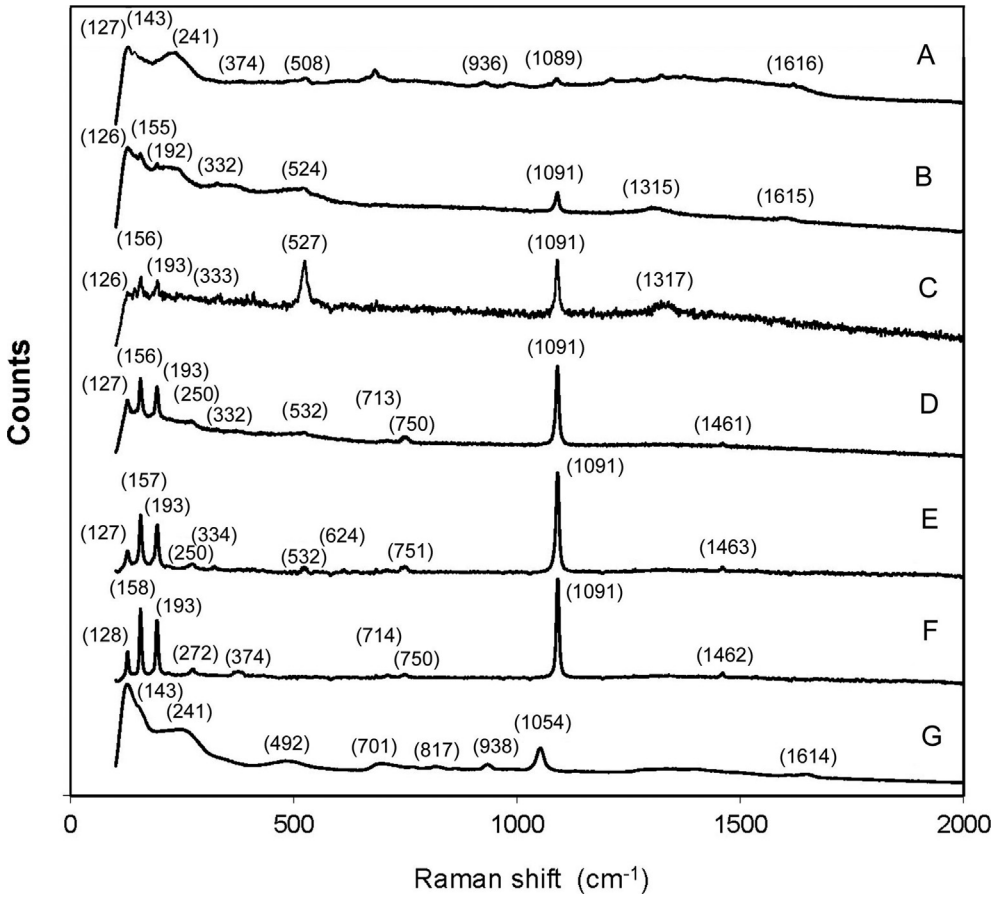

Fig. 9. Raman spectrum for different unbaked cathode mixtures: (A) mixture 22%Li_2O + 78%Ag where Li_2O is produced by burning metallic Li; (B) mixture 22%Li_2O + 78%Ag where Li_2O is commercial powder; (C) Li_2O powder; (D) mixture 18%LiOH + 82%Ag; (E) LiOH powder; (F) Li_2CO_3 powder and (G) silver powder.

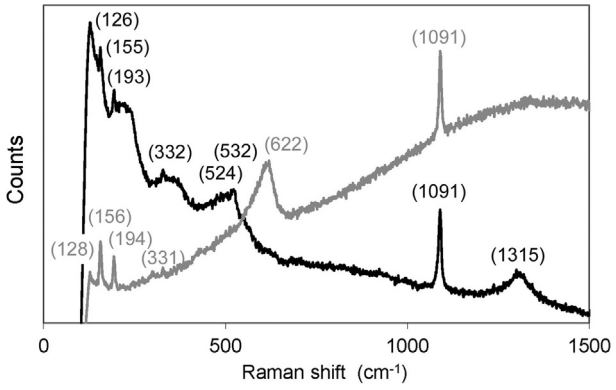

Fig. 10. Raman spectrum for unbaked (black) and baked (grey) cathode mixtures of 22% Li_2O + 78%Ag using Li_2O commercial powder.

3. Results

The fine powder composition depended strongly on the mixing technique as shown in optical images (Fig. 4) produced by different methods.

During pressing, the relationship between the volumes occupied by a powder versus the force needed to attain this volume, was used to assess the mechanical properties of the mixture. The scale on the dial gauge was chosen so that the readings decreased as the load was applied to the die, therefore the experimental data took the form shown in Fig. 5.

3.1. Performance of different cathode mixtures

An analysis of typical negative ion spectrum from different cathode mixtures is presented in Table 4. In all experiments the total output of negative current was about 15 μA.

Pressed samples were analysed using SEM, as shown in Figs. 6–8. Mixed secondary electrons (SE) and back-scatter electrons (BSE) images gave an indication of the size of powder particle distribution, topography and composition on the surface of the sample.

The results of qualitative EDX analyses of the elements present in different cathode mixtures are given in Table 5.

Raman spectra collected from different unbaked cathode mixtures are shown in Fig. 9. Depicted in Fig. 9A and B are the Raman spectra of 22%Li_2O + 78%Ag using burnt metallic lithium and commercial Li_2O powder respectively. For reference, Raman spectrum of Li_2O powder is also shown in Fig. 9C. In most cases, baked samples were not Raman analysed due to high fluorescence backgrounds.

Fig. 9D and E show LiOH spectra with and without Ag binder respectively. Raman spectra of lithium carbonate Li_2CO_3 and silver powder are shown in Fig. 9F and G. The observed Raman bands at 127, 156, 192, 271, 374, 508, 711, 748, 1090 and 1459 cm^{-1} were assigned to Li_2CO_3 and were comparable with those reported previously [25–27]. The LiOH and Li_2O exhibited their characteristic Raman bands at 334, 624 cm^{-1} [28,29] and 523, 528, 1316 cm^{-1} [30–32] respectively. The peaks with wave number 250 and 533, Fig. 9D, E were assigned to $LiOH{\cdot}H_2O$ as reported in [29]. In case of pressed silver powder, Fig. 9G, the assignment of the bands at 143, 241, 492, 701, 817, 938, 1054 and 1614 cm^{-1} were tentative [33]. Some unmarked peaks were from fluorescent light spectrum as it appeared for 785 nm laser.

Raman spectra, for unbaked and baked cathode mixtures of 22% Li_2O + 78%Ag using commercial Li_2O powder, are displayed in Fig. 10. The spectrum for the unbaked mixture was the same as shown in Fig. 9B. In Fig. 10 it was superimposed on the spectrum for the same specimen after bake out. The spectrum for the baked sample (grey

Table 6
Observed Raman shifts of lithium carbonate, lithium hydroxide, lithium oxide, silver and silver oxide.

Compounds	Raman shift, cm^{-1}										References
Li_2CO_3	127	156	192	271	374	508	711	748	1090	1459	[25–27]
	128	157	194	272	374	508	714	751	1091	1463	#
LiOH	334	624									[28,29]
	331	622									#
Li_2O	523	528									[30–32]
	524	527								1315	#
$LiOH·H_2O$	121	149	219	251	401	533	851			3572	[29]
				250		531					#
Ag_2O Ag/Ag_2O	143	230–248		487			933–950		1072		[33]
	143	241		492	701	817	938		1054	1614	#

Figures that appear in this work.

colour) was masked by strong fluorescence.

The frequencies of all Raman bands observed in this study, along with published reference values, are summarised in Table 6.

4. Discussion

A certain amount of crushing and grinding were required to decrease the particle size of powders and improve homogeneity as shown in Fig. 4. The effect of grinding (Fig. 4d) compared to mixing by spatula (Fig. 4b) was more visible at the edge of the cathode die, where the powder was undisturbed by punch movement.

During the initial stage of fragmentation and plastic deformation shown in Fig. 5, the volume of powder rapidly reduced with applied force until contact points between powder particles became established. The second stage was characterised by sharp decrease in the rate of volume reduction, caused by elastic deformation as the force continued to rise (Fig. 5). For majority of applications, the applied force was limited to a maximum of 1 ton. At a punch diameter of 3.3 mm, this force corresponded to a die pressure of 1.15 GPa. This was well above the copper ultimate tensile strength of 210 MPa. However, the external steel housing was able to contain the copper cathode. Since the cathode blank had internal cavities, Fig. 1, failure due to shear loads was a concern. The maximum measured shear load that caused plastic deformation of the die was observed at applied force of 2.4 tonnes or 2.75 GPa.

In case of burnt Li metal, both unbaked and baked samples performed similarly, producing ~μA negative Li^- beam with high efficiency in the order of 4–5% of the total source current, as shown in Table 4. In the baked samples, less OH^- and higher C^- fractions were produced. All samples exhibited segregation of main components from the silver binder after bake out shown in Figs. 6–8. This resulted in formation of silver-poor and silver-rich regions confirmed by EDX analyses (Table 5). The chemical compositions measured by EDX and Raman spectroscopy did not contain LiOH, which contradicted previous findings [16]. Qualitative EDX analyses of burnt lithium samples showed higher concentrations of C and the presence of N after bake out (Table 5). Raman spectra collected from burnt lithium metal showed mainly Li_2CO_3 and silver (Fig. 9A, G and Table 6). Good performance from burnt lithium samples could be attributed to the following: (i) the main component of the mixture was Li_2O, characterised by moderate value of enthalpy of formation (Table 3), and (ii) due to low content of absorbed water through within the sample. The water molecules have low bond-dissociation energy of 268 kJ/mol. Moreover, the hydrogen atom H and hydroxyl radical OH have high electron affinities (see Table 4) as compare to Li atom. Therefore, in the presence of moisture, the production of large fluxes of H^- and OH^- due to ion-enhanced desorption from the surface of the cathode is likely to have suppressed the negative lithium beam formation [24].

Baked mixtures based on Li_2O performed much better, producing Li^- ion beams up to 4.4% of the total source current compared to only 1.6% for unbaked samples (Table 4). Similarly, baked samples produced less yield of H^-, OH^- and higher C^- currents indicating lower concentrations of moisture and higher amounts of lithium carbonate, consistent with EDX analyses (Table 5). Raman spectra for unbaked mixtures 22%Li_2O + 78%Ag (Fig. 9B) and Li_2O powder (Fig. 9C) contained bands corresponding to Li_2O, LiOH and Li_2CO_3 (Table 4). The band for Li_2O 523 cm^{-1} was broad, overlapping with the 533 cm^{-1} band as reported for $LiOH·H_2O$. The $LiOH·H_2O$ band 533 cm^{-1} disappeared after the samples were baked and the LiOH band reappeared at 622 cm^{-1} (Fig. 10), suggesting that the lithium hydroxide-monohydrate dehydrated and partially transformed to LiOH. As discussed earlier, the presence of absorbed water in lithium hydroxide- monohydrate could explain the low negative lithium beam outputs in unbaked samples.

In case of LiOH, the baked sample's performance was much better, generating a negative Li^- beam output ~11.0% of the total source current compare to 1.0% for unbaked sample (Table 4). The baked sample produced slightly higher currents of H^-, OH^- in spite of the absence of water molecules. Both negative hydrogen ions and hydroxide ions could be produced from hydroxyl radical generated by bond dissociation of LiOH molecular. Likewise, only marginally higher current of C^- was measured, which was not consistent with the expected carbon content based on EDX analyses (Table 5). Raman spectra for the unbaked 18%LiOH + 82%Ag mixture (Fig. 9D) and LiOH powder (Fig. 9E) contained bands corresponding to LiOH, $LiOH·H_2O$ and Li_2CO_3 (Table 6). Despite acceptable source output, the Li^- current was unstable and the high sputtering rate of the cathode mixture indicated poor ionization efficiency. In addition, the mechanical integrity of the pressed powder under ion bombardment was not satisfactory.

Finally, in the case of lithium carbonate cathode mixture, its low solubility in water relative to other lithium salts meant that it was insensitive to baking. Similar outputs of Li^- beam were observed for baked and unbaked samples. In both cases, the negative lithium beam output was quite poor, about 1.5% of the total extracted current, which was in disagreement with findings reported in [17]. This was probably due to the high value of standard enthalpy (heat) of formation of Li_2CO_3, −1215.6 kJ/mol, Table 3.

5. Conclusions

A variety of lithium-based chemical compositions have been used in the cathode of caesium sputter-type ion source to generate high intensity negative lithium-ion beams. The best results have been achieved with burnt lithium metal and commercial lithium oxide as base components. With lithium oxide, the moderate bake out of the cathode in air is an essential preparation step in order to achieve good performance. In all cases, the presence of water is the main cause of poor performance due to formation of large concentration of H^- and OH^-

which suppress the output of the negative lithium beams. Additional data is required to investigate the cathode degradation during long term storage in ambient conditions, as well as investigating the different settings of bake-out and powder mixing, such as duration and temperature. An alternative sample preparation technique, based on bake out of powder mixture before pressing and choice of alternative binding components, will be further explored.

Acknowledgement

This work has been supported by Australian Federal Government Superscience/EIF funding under the NCRIS mechanism. We acknowledge access to NCRIS facilities (ANFF and the Heavy Ion Accelerator Capability) at the Australian National University. I would like to thank J. Ashenfelter, Dr. P. Tikkanen, D. Ovidiu, J. McKay, D. Steski, J. Carlos de Abreu, Dr. L. Gasques, L. Lamm and other colleagues through SNEAP network who have helped with fruitful discussions and provided valid material for the paper. The author wishes to express his appreciation to RSPE's Nuclear Physics technical staff members Dr. P. Linardakis, T. Tunningley, S. Battison, D. Tsifakis, J. Bockwinkel, B. Tranter, B. Graham and J. Heighway. Special thanks are due to Dr. M. Lockrey for expert support in SEM/EDX analyses. Dr. L. Smillie is specially thanked for his help with Raman characterisation.

Appendix A. Supplementary data

Supplementary data associated with this article can be found, in the online version, at http://dx.doi.org/10.1016/j.nimb.2017.11.004.

References

[1] G.D. Dracoulis, Trends in nuclear structure with heavy ions, Nucl. Instrum. Methods Phys. Res., Sect. A 382 (1996) 1–19.
[2] G.K. Mehta, Material modification with high energy heavy ions, Nucl. Instrum. Methods Phys. Res., Sect. A 382 (1996) 335–342.
[3] K. Betge, Alpha-particle transfer reactions, Annu. Rev. Nucl. Sci. 20 (1970) 255–263.
[4] D.H. Luong, M. Dasgupta, D.J. Hinde, R. du Rietz, R. Rafiei, C.J. Lin, M. Evers, A. Diaz-Torres, Insights into the mechanisms and time-scales of breakup of ^{6,7}Li, Phys. Lett. B 695 (1–4) (2011) 105–109.
[5] H. Baumann, K. Bethge, E. Heinicke, Production of negative lithium ions in a Penning discharge, Nucl. Instrum. Methods 46 (1967) 43–44.
[6] M. Re, M. Menna, F. Chines, G. Cuttone, E. Messina, D.W. Stracener, J.C. Bilheux, The production of negative lithium beams by charge exchange in caesium vapours, in: Proc. of 2005 Particle Accelerator Conference, Knoxville, Tennessee, USA, 2005, pp. 898–900.
[7] R. Middleton, A review of negative ion sources, Nucl. Instrum. Methods 233 (1984) 1435–1444.
[8] R. Middleton, A versatile high intensity negative ion source, Nucl. Instrum. Methods 214 (1983) 139–150.
[9] J.H. Billen, Emittance calculations and measurements for a sputter-type negative-ion source, Nucl. Instrum. Methods 220 (1984) 225–250.
[10] G.D. Alton, J.W. McConnell, The emittances and brightness of high-intensity negative ion sources, Nucl. Instrum. Methods Phys. Res., Sect. A 268 (1988) 445–455.
[11] A. Nadji, F. Haas, G. Heng, Ch. Muller, R. Rebmeister, The beam emittance of negative ion sources, Nucl. Instrum. Methods Phys. Res., Sect. A 287 (1990) 173–175.
[12] J. Southon, G.M. Santos, Life with MC-SNICS. Part II: further ion source development at the Keck carbon cycle AMS facility, Nucl. Instrum. Methods Phys. Res., Sect. B 259 (2007) 88–93.
[13] A. Priller, M. Auer, R. Golser, A. Herschmann, W. Kutschera, J. Lukas, P. Steier, A. Wallner, Ion source refinement at VERA, Nucl. Instrum. Methods Phys. Res., Sect. B 259 (2007) 94–99.
[14] P.A. Hausladen, D.C. Weisser, N.R. Lobanov, L.K. Fifield, H.J. Wallace, Simple concepts for ion source improvement, Nucl. Instrum. Methods Phys. Res., Sect. B 190 (2002) 402–404.
[15] D.C. Weisser, N.R. Lobanov, P. Hausladen, K. Fifield, H. Wallace, S. Tims, E. Apushkinsky, Novel matching lens and spherical ionizer for a caesium sputter ion source, Pramana 59 (6) (2002) 997–1006.
[16] R. Middleton, A negative-ion cookbook, Department of Physics, University of Pennsylvania, Philadelphia, 1990, available at http://www.albany.edu/ionbeamlab/downloads/NegativeIonCookbook.pdf (accessed on May 17th, 2017).
[17] G.D. Alton, G.D. Mills, Production of atomic ion beams of the group IA elements, in: Proc. Symposium of North Eastern Accelerator Personnel, Yale University, USA, 1988, pp.161–167.
[18] The Symposium of Northeast Accelerator Personnel (SNEAP) discussion forum, available at http://www.tunl.duke.edu/~sneap/ (accessed on May 17th, 2017).
[19] P.J. Denny, Compaction equations: a comparison of the Heckel and Kawakita equations, Powder Technol. 127 (2) (2002) 162–172.
[20] M. Schiemann, J. Bergthorson, P. Fischer, V. Scherer, D. Taroata, G. Schmid, A review on lithium combustion, Appl. Energy 162 (2016) 948–965.
[21] C.O. Willits, Methods for determination of moisture oven drying, Anal. Chem. 1058 (1951) 23.
[22] C.A. Jacobson, Encyclopedia of Chemical Reactions vol. IV, Reinhold Publishing Corporation, NY, 1959.
[23] R. Behrisch, G. Bets, G. Carter, B. Navinsek, J. Roth, B.M.P. Scherzer, P.D. Townsend, G.K. Wehner, J.L. Whitton, Sputtering by Ion Bombardment II, Springer-Verlag, Berlin, 1983, pp. 11–84.
[24] J.S. Vogel, Anion formation by neutral resonant ionization, Nucl. Instrum. Methods Phys. Res., Sect. B 361 (2015) 156–162.
[25] P. Pasierb, S. Komornicki, M. Rokita, M. Rekas, Structural properties of Li_2CO_3-$BaCO_3$ system derived from IR and Raman spectroscopy, J. Mol. Struct. 596 (2001) 151–156.
[26] N. Koura, S. Kohara, K. Takeuchi, S. Takahashi, L.A. Curtiss, M. Grimsditch, Marie-Lousie Saboungi, Alkalai carbonates: Raman spectroscopy, ab initio calculations and structure, J. Mol. Struct. 382 (1996) 163–169.
[27] M.H. Brooker, J. Wang, Raman and infrared studies of lithium and cesium carbonates, Spectrochimica Acta 48A (7) (1992) 999–1008.
[28] F. Harbach, F. Fischer, Raman spectra of lithium hydroxide single crystals, J. Phys. Chem. Solids 36 (1975) 601–603.
[29] V.I. Tyutyunnik, Lithium hydroxide monohydrate single crystals: infrared reflectivity and Raman study, J. Raman Spectrosc. 31 (2000) 559–563.
[30] Y. Ishi, T. Nagasaki, H. Watanabe, H. Ohno, Temperature dependence of the Raman spectrum in lithium oxide single crystal, J. Am. Ceram. Soc. 74 (9) (1991) 2324–2326.
[31] T. Osaka, I. Shindo, Infrared reflectivity and Raman scattering of lithium oxide single crystals, Solid State Commun. 51 (6) (1984) 421–424.
[32] R.S. Sanchez-Carrera, B. Kozinsky, Computational Raman spectroscopy of organometallic reaction products in lithium and sodium-based battery systems, Phys. Chem. Chem. Phys. 16 (2014) 24549–24558.
[33] I. Martina, R. Wiesinger, D. Jembrih-Simburger, M. Schreiner, Micro-Raman characterisation of silver corrosion products: instrumental set up and reference database, e-preservation, Science 9 (2012) 1–8.